Chapter 11
Magnetic Resonance as a Tool for Pharmaco-Imaging

Brian R. Moyer, Tom C.-C. Hu, Simon Williams, and H. Douglas Morris

Abstract Imaging technologies in the nonclinical laboratory have been greatly bolstered by the ever-improving methods available with magnetic resonance (MR) imaging. Small animal systems have been growing in capability even while becoming more amenable to use by biologists, revolutionizing how we can study pathophysiology and follow a drug or biologic therapy. MR's ability to characterize many anatomical and physiological processes, based on their underlying influence on tissue magnetization properties, has led, for example, to discoveries in the psychopharmacology of attention deficit and cognitive drug therapies and in recording changes of oxygenation, blood flow and vessel permeability in acute studies, or the chronic remodeling of tissue water diffusion following therapy. This is a short and clearly abbreviated discussion of the applications of MRI in the nonclinical

B.R. Moyer, M.S. (Pharm), M.S. (Tox), C.N.M.T. (✉)
BRMoyer & Associates, LLC, 23 Hawk Drive, Bedford, NH 03110, USA
e-mail: bmoyernh@gmail.com

T.C.-C. Hu, Ph.D., M.B.A.
Health and Human Services (HHS), Office of the Assistant Secretary for Preparedness and Response (ASPR), Biomedical Advanced Research and Development Authority (BARDA), Washington, DC 20201, USA

Nuclear and Radiological Engineering/Medical Physics Program, George W. Woodruff School of Mechanical Engineering, Georgia Institute of Technology, North Avenue, Atlanta, GA 30332, USA
e-mail: tom.hu@hhs.gov

S. Williams, D.Phil.
Department of Biomedical Imaging, Genentech, Inc., 1 DNA Way, South San Francisco, CA 94080, USA
e-mail: williams.simon@gene.com

H.D. Morris, Ph.D.
NIH Mouse Imaging Facility, National Institute of Neurological Disorders and Stroke, National Institutes of Health, 10 Center Drive, B1D-69, Bethesda, MD 20892, USA
e-mail: dmorris@nih.gov

B.R. Moyer et al. (eds.), *Pharmaco-Imaging in Drug and Biologics Development*,
AAPS Advances in the Pharmaceutical Sciences Series 8, DOI 10.1007/978-1-4614-8247-5_11,

(and clinical) drug development laboratory, and it is meant to introduce the reader to the concepts and how this specific imaging modality likely offers the most versatile of all imaging modalities as well as being one with very high resolution.

Abbreviations

ADC	Apparent diffusion coefficient—the diffusion of molecules in tissues is modulated by many mechanisms that restrict or impose tortuosity around obstacles and such as blood flow in small vessels or cerebrospinal fluid in ventricles and other contributions to MR signal attenuation. Images are "weighted" by the "apparent" diffusion processes. Note that the ADC concept has been extremely successful in tumor biology to demonstrate necrosis, especially for clinical applications. The basic ADC approach has been challenged recently, as new, more comprehensive models of diffusion in biological tissues have been introduced. Also, the rADC, or relative ADC, is a ratio of lesions to control brain ROIs
B_0	Static main magnetic field provided by the MR system magnet
B_1	Secondary magnetic field perpendicular to B_0 transiently created during an experiment by the system's radiofrequency coils and gradient sets
BOLD	Blood oxygen level dependent (a particular contrast mechanism)
Chemical shift	The resonant frequency of nuclei in some chemical environment relative to those in a standard environment (e.g., the protons of benzene)
CNR	Contrast-to-noise ratio—the CNR is directly linked to statistical measures such as the *t*-values, but it does not depend on the number of points or runs as do the *t*-values; in fMRI it is made up of the functional signal change and the temporal signal change as the average signal change (task related) over the non-task-related variability over time (time-series noise)
FT	Fourier Transform—a mathematical treatment of the FID or echo signal from a modern pulsed MR experiment to convert the recorded time-domain data into usable spatial frequency-domain data and hence images; an MR image consists of a matrix of pixels based on the number of lines filed in "K-space" (phase matrix) and the number of data points in each line (frequency matrix)
FID	Free induction decay—the signal observed during the process of relaxation that follows an excitation of nuclei induced by a pulse of radiofrequency energy
FOV	Field of view—physical dimensions of the imaged volume

fMRI	Functional magnetic resonance imaging—generally for cerebral blood flow
Gradient	A (relatively small) magnetic field that increases in strength with distance from the center of the image; these are created transiently by pulses from the gradient coils to impart the magnetic spins with frequency and phase information to facilitate image formation
K-space	A spatial frequency domain where information on the frequencies of a signal and where it comes from (on the gradient) in the patient is located; this information is in radians per cm; often called the chest of drawers for how the data is stored
NMR	Nuclear magnetic resonance—general term for the analytical chemistry of chemical shift analysis and the former term of MR as "NMR imaging"
phMRI	Physiologic or pharmacologic imaging using MRI
Pulse sequences	A programmed sequence of magnetic field pulses and time delays from the radiofrequency coil and the gradient set during the imaging experiment which manipulate the spin behavior of nuclei; changes to the induction and relaxation can be exploited to reveal properties of the tissue of interest
Relaxation	Process by which a population of excited (high-energy) nuclei give up RF energy and return to their ground (low-energy) state. This emitted energy is detected to form the images
Relaxivity	The ability of magnetic compounds to increase the relaxation rates of the surrounding water proton spins. Relaxivity is used to improve the contrast of the image and to study tissue-specific areas where the contrast agent better diffuses; view http://www.youtube.com/watch?v=Osx8Ced9Eyw
RF	Radiofrequency—the resonant frequency of protons at commonly used magnetic field strengths is in the radiofrequency range, e.g., 64 MHz at 1.5 Tesla
SNR	Signal-to-noise ratio
T_1	Longitudinal relaxation occurs when a population of excited nuclei give up their extra energy to the surrounding electronic environment; the time constant "T_1" (63 % of the longitudinal magnetization to recover) for this process is also known as the "spin–lattice" relaxation time constant. T_1 values are typically on the order of a second
T_2	Transverse relaxation occurs when a population of excited nuclei exchange energy with their neighbors; the time constant "T_2" (63 % of the longitudinal magnetization to recover) for this process is also known as the "spin–spin relaxation" time constant. In biological tissues T_2 values are typically on the order of tenths of a second

T_2*	The observed decay of the FID signal following the RF excitation pulse; it is faster than T_2 as it is the combination of the T_2 decay superimposed on dephasing phenomena such as magnetic field inhomogeneity
Tesla	One weber per meter squared; the SI unit of magnetic field strength
TOF	Time of flight—flowing nuclei present in a slice of interest which has an excitation pulse applied; more or less signal is recovered depending on their velocity; useful in magnetic resonance angiography
	A full listing of definitions is available at http://cis.rit.edu/htbooks/mri/gloss.html (8 pages of glossary terms)

11.1 Introduction to Magnetic Resonance Imaging

The field of modern biomedical imaging has been heavily influenced by the maturation of nuclear magnetic resonance (NMR) away from its roots as an analytical chemists' spectroscopic tool into the medical application known as magnetic resonance imaging (MRI). As a disclaimer we must acknowledge that this chapter cannot even begin to teach all the fundamentals of MR chemistry, physics, and mathematics nor even biology; MR is a field in its own right. For an excellent treatise with full coverage of the topic of magnetic resonance imaging and excellent illustrations of the physics, instrumentation and equipment imaging techniques and examples of various imaging artifacts, and safety, we refer the reader to the book entitled *MRI in Practice* by Westbrook, Roth, and Talbot (4th Ed., 2011, a Wiley-Blackwell publication).

The role of magnetic resonance imaging in drug development has grown exponentially as the instrumentation has become more refined, more widely available, and easier to use. This has been driven in part by the rapidly expanding clinical utility of MRI and the prospect of having a bench-to-bedside translation for many important experiments. Wise and Tracey (2006) have provided a comprehensive view of how one aspect of MRI, functional MRI (fMRI), is being used in drug development, specifically in brain functional assessments under drug challenges and therapies. More will be discussed on fMRI in the field of psychotherapy and neuropharmacology in a later section. It is the premise of this book that imaging has over the past 50–60 years advanced the portfolio of imaging agents, contrast agents, and other imaging probes and has begun the new exploitation of biomarkers—elements of physiologic expression—using the many radiotracers, US-CT-MR contrast agents, optical probes, and more and the imaging platforms of CT and MR as tools to dissect disease. We have an armament of tools at our disposal and one of the most versatile is magnetic resonance imaging. Advances in phMRI (physiologic MRI) are making huge strides in our understanding of drug effects on brain function, tumor susceptibility to novel therapeutics, cardiac imaging and blood/vascular

imaging (especially in stroke and deep vein thrombosis, or DVT), and even lung function such as pulmonary fibrosis and ventilation.

Modern clinical radiological imaging relies on the existence of useful image contrast between tissue types. Even before the field of MRI was developed, alterations were noted in the spin–lattice (T_1) and spin–spin (T_2 and T_2*) relaxation times of solutions containing paramagnetic ions. The significance of this alteration for the development of MRI was that small differences in the local magnetic properties of substances could be detected in spectroscopic changes of the surrounding water. In particular, Damadian observed that the relaxation times for tumors in rats presented differently than normal tissue as a function of the decrease in water constrained in tumor tissue (Damadian et al. 1977; Geva 2006). In a 1973 seminal paper, Paul Lauterbur demonstrated spatial localization via NMR, which he called "zeugmatography," and the utility of relaxometry in imaging. The first images were of two capillary tubes in a NMR spectrometer (Lauterbur 1973). One capillary contained a solution of $MnSO_4$ in order to reduce the T_1 of the observed hydrogen nuclei in water. By increasing the power of the RF transmission, two different images ("zeugmatograms") were acquired, which showed variation in the image intensity for the $MnCl_2$ solution capillary compared to water only, and demonstrated the feasibility of using T_1 variation as an image contrast. Lauterbur further postulated that all NMR visible phenomena, such as chemical shifts, diffusion, and dipolar couplings, can be "visible" in an image form.

As illustrated in the example above, intrinsic relaxometric differences in tissue can serve as image contrast, and furthermore, contrast can be enhanced by agents with different affinities for pathological and healthy tissue. Useful qualities of a contrast agent include (a) physical properties that affect the local magnetic environment sensitively and (b) chemical properties that allow the contrast agent to travel to the appropriate region of interest for imaging. MRI continues to be dominated by detection of the protons in tissue water, and our discussion will focus on these widespread ^{1}H MR techniques. However, we note that MRI with less common nuclei such as ^{23}Na or ^{19}F have been investigated and may have niche roles to play in fields such as imaging brain function or tissue oxygenation, respectively.

11.1.1 Pulse Sequences

Pulse sequences are the tools of the MRI imaging scientist. They can be thought of as a way to "sculpt" or "paint" the images using a wide variety of "paint brushes." These sequences are a series of RF pulses and magnetic field gradient applications spaced at carefully defined intervals so that the whole sequences excite or rephrase the resonance response following field perturbation. One "paints" with alterations in pulses and gradients. The brushes are simply how we address and make the RF pulses interact with the magnetic field both temporally and spatially. There are many pulse sequences in practice, and they each take some knowledge of the pathology of interest to select and customize appropriately; there may not be a single choice that is optimal.

Table 11.1 describes some frequently encountered pulse sequences, their most common abbreviations, and basically what they are directed to do in the generation of an image. Each pulse sequence is designed to accomplish a specific purpose, such as eliminating signal from static structures to reveal motion; this is not always to create a "better" image, but rather to improve image quantification and to emphasize particular aspects of the physiology being studied. The advantages and disadvantages of each pulse sequence are too complex to cover in this chapter; however, the reader is invited to review the textbook of Westbrook, Roth, and Talbot, *MRI in Practice*, published by Wiley-Blackwell, 2011 (Chap. 5 in the 3rd edition). Another textbook to review, especially for small animal imaging examples, is *Practical Small Animal MRI*, also published by Wiley-Blackwell by Gavin and Bagley (2009).

11.1.2 Potential Uses of MRI for Pharmaceutical Imaging

The pharmaceutical industry has for years investigated drug and biologics in development by measuring changes intrinsic to the physiologic behavior of the systems being targeted, such as the receptor-mediated generation of a biochemical signal that leads to some behavioral, functional, biochemical, or biophysical change to the system. MR imaging takes full advantage of the later phenomena, with the relaxation properties of tissue water greatly influenced by subtle variations in the presence of blood, oxygen, lipid membranes, proteins in solution or in aggregates, the anisotropic orientation of nerve fibers, etc. The intrinsic behavior of hydrogen (a dipole magnet in itself with a POS proton and a NEG electron forming a dipole; essentially encumbered as water) can be mapped in biophysical terms and exploited to create a signal of metabolic change (chemical exchanges in a chemical reaction, e.g., magnetic resonance spectroscopy; see Chap. 12 of this book) or as an anatomic change (tissue-type transitions and edge detection) and even as a measure of flow as magnetized blood elements flow through a tissue. Each of these behaviors allows an investigator to use nonionizing electromagnetic fields (B_1) in a magnetic field (B_0) to interrogate biologic systems. On top of this rich variety of intrinsic tissue contrast are all the additional contrast mechanisms available to us through the introduction of extrinsic contrast agents. We commonly apply contrast agents in CT and X-ray imaging, but contrast agents can also be used to enhance MRI. Contrast agents differ from radioactive tracers (say) in that they are not detected by the system directly but rather by their alteration of the local magnetic fields and the resultant change in resonant frequency (chemical shift) or relaxivity, properties which can be differentiated with an appropriate pulse sequence.

The magnetic properties of tissue and even contrast agents vary with the magnetic field strength. Higher field strengths lead to inherently higher detection sensitivity because a greater net polarization of the nuclear spins is achieved, but this comes with the potentially unwelcome complications of increased T_1 and decreased T_2 relaxation times which makes it more difficult to maintain (and image) transverse magnetization, adversely affecting the use of pulse sequences with long echo trains

Table 11.1 Pulse sequences, abbreviations (common—manufacturers may use different acronyms for the same sequence, refer to the manufacturer terms of use), mechanisms, and purpose

Pulse sequence name	Abbreviations	Purpose
Spin-echo types		
Conventional	SE	The "gold standard" In general, T_1 for anatomy and T_2 for pathology (tissues that are diseased may have more edema or vasculature)
Fast or turbo	FSE, TSE	A spin-echo scan with shorter scan times; by virtue of how it fills K-space it is useful in "stationary" organ systems; not so useful in chest, or abdomen (K-space will be defined for the reader in the next section)
Inversion recovery	IR	Good for accurate T_1 measurements and contrast on low-field systems
Fast inversion recovery	FIR	A modification of IR where multiple lines of K-space are filled as in FSE
Short tau inversion recovery	STIR	Important in musculoskeletal imaging as bone marrow and bruising are suppressed as well as fat
Fluid attenuated inversion recovery	FLAIR	Useful for attenuating signal from CSF in brain and spinal imaging to emphasize periventricular and spinal cord injuries
Gradient echo types		
Conventional	GE	Variable flip angles so that the TR (and scan time) can be reduced; used for T_2* and T_1 and proton density weighted images; sensitive to flow and thus useful for angiography
Steady-state/echo formation	SSEF	Steady state = TR is shorter than the T_1 or T_2 relaxation times (no time for transverse magnetization to occur); steady state sequences have high signal when T_1/T_2 ratios approach 1.0)
Coherent gradient echo	GRASE, FFE, FISP, FAST	Coherent = residual transverse magnetization (from previous RF pulses) is in phase; rapid images of T_2* weighted; used for vessel patency assessments or fluid (cystic) identity
Incoherent gradient echo (or spoiled)	SPGR, T_1FFE, FLASH	Incoherent = residual transverse magnetization (from previous RF pulses) is out of phase; RF spoiled pulses product T_1 or proton density images; useful T_1 anatomy with Gd contrast

(continued)

Table 11.1 (continued)

Pulse sequence name	Abbreviations	Purpose
Steady-state free precession	SSFP	Used for true T_2 weighting; brain and joints for 2D and 3D volumetric imaging; fast spin echo (FSE), however, is often a better choice as it has better T_2 weighting plus short scan times
Balanced gradient echo	BGE	Modified coherent gradient echo; corrects for rephasing in flowing blood; imaging the heart and great vessels and spinal images, especially the auditory meatus and cervical spine reservoirs
Fast gradient echo	FGE	Single breath-hold technique for very fast pulse sequences and volume acquisitions; multiple slices in respiratory scans, esp. dynamic contrast enhanced lung lesions; also for the abdomen and the breast
Echo planar imaging	EPI	A method that collects all the data required for a full K-space acquisition and from a single echo train. Very efficient at low magnetic field strengths and widely used in clinical imaging. But it is technologically very demanding on the hardware since filling K-space in this situation requires rapidly and continuously slewing the readout gradients. Can be combined with "magnetization preparation" pulses to create a variety of alternative relaxation images. Safety can be an issue with rapid gradient switching leading to nerve stimulation. EPI becomes difficult at higher fields due to distortion and chemical shift artifacts
Parallel imaging techniques		
Parallel imaging	ASSET, SENSE, iPAT, SMASH	Sensitivity encoding; fills K-space efficiently by multiple lines acquired via coupled coils enabled to acquire data simultaneously; systems are available with 2, 4, 6 and 8 coil couplings can be employed. Requires advanced hardware but an important technique that shortens scan times but may suffer from chemical shift artifacts from mismatched resonant coil frequencies

like EPI and altering the impact of contrast agents. Because building magnets with higher field strengths or larger diameters is relatively expensive, magnets which have to be large enough to accommodate human patients typically operate at lower field strengths (0.5–3 T) than those commonly found in small animal imaging laboratories (4.7–11 T). Very high-field magnets, such as the 21.1 T system at the National High Magnetic Field Laboratory in Florida, help to quantify the benefits and challenges that come with increasing field strength, and some clinical research centers have magnets of 9.4 T and higher. Because rapid imaging with EPI and the use of contrast-enhancing agents are important for some applications, and this is easier to achieve at relatively low fields such as 1 T, a new generation of relatively affordable low-field small animal imaging systems is being made available by manufacturers traditionally associated with high-field magnets, such as Bruker. Exploration of small animal imaging at field strengths beyond 9.4 T is mostly of academic interest at present but is very much application-dependent. Other technological developments also aim to increase the sensitivity of the MR experiment, such as more precise RF electronics, low-noise detector design, especially with cryogenic cooling of the RF coil and receiver electronics, and the design of coils with application-specific forms for maximum efficiency such as the multi-element spine coils common in the clinic and now being implemented in small animal systems. These developments may offer sensitivity improvements at lower cost and with fewer consequences than continually increasing the magnetic field strength.

Fundamental questions facing drug and biologics developers when testing a NCE into an animal model for advanced development may be answered using imaging applications. The listing below (and this list is certainly not exhaustive) addresses some imaging points about inclusion of an imaging approach to development questions:

- MR, like CT, addresses anatomy and distortions of anatomy very well (see Chap. 7 in oncology).
- Also, like CT, disease model natural history progression (i.e., tumor growth and RECIST determination) assessment is possible but with a distinct advantage in chemical characterization, such as discriminating lean from fatty tissues.
- Risk of different drug/biologic activities related to circadian rhythms may be imaged (i.e., neurologic changes in day–night sleep patterns and even hibernation).
- Biologic signal response times: Long duration versus immediate measures.
- Blood flow in tumors, angiogenesis, chemotherapeutic, and radiation effects.
- Appropriateness of use of multimodal imaging reagents/platforms.
- *Cell therapies*: Methods for labeling of cells ex vivo and in vivo and methods to follow stem cell tracking.
- Noninvasive imaging of proliferation and necrosis; histologic slice correlates.
- Changes in metabolic activity (and with circadian rhythms).
- Choosing the appropriate functional and/or quantitative platform.
- *Lung*: Noninvasive imaging of oxidative stress and lung function/fluid clearance, volume changes, capacity, macrophage activity, and changes in compliance due to fibrotic changes.

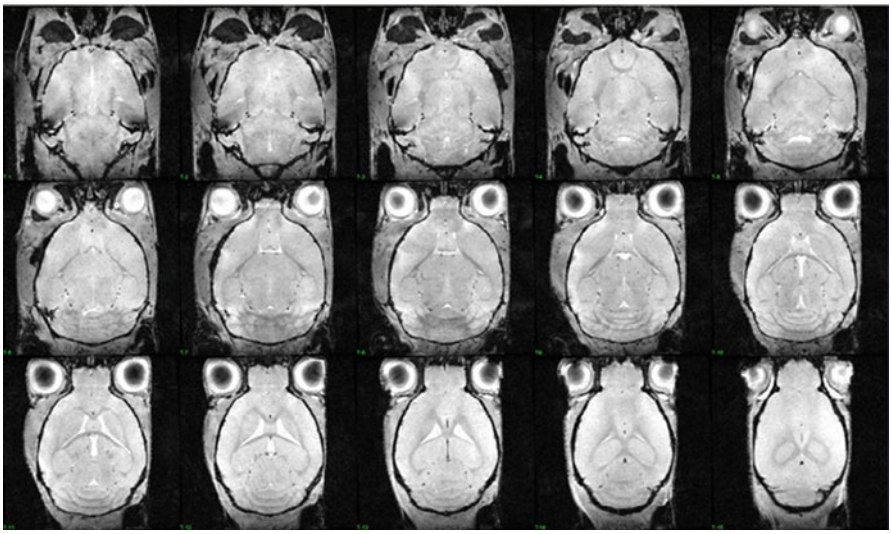

Fig. 11.1 Depiction of the mouse brain from the floor of the cranium (*upper left*) to the superior aspect above the ventricles (*lower right*) using a very high-magnetic-field system. From: Florida State University, National High Magnetic Field Laboratory using their 900 MHz system at 62×62 micron resolution in 150 micron slices; Resources include: Initial in vivo rodent sodium and proton MR imaging at 21.1 T. Schepkin VD, Brey WW, Gor'kov PL, Grant SC. *Magn Reson Imaging*. 2010; 28(3):400–407. With permission. http://www.magnet.fsu.edu/usershub/scientificdivisions/nmr/probes/probe_900mri.html

- *Kidney/liver*: Renal blood flow, clearance of drugs based upon renal function, liver metabolic changes, biliary flow, blood flow, tubular secretion.
- *GI tract*: Drug dissolution, segmental analysis/function, GI transit time, blood flow, crypt and villus apoptosis, GI lesions of various etiologies.
- *Wound* healing: Hematopoietic trafficking, clotting, stem cell arrival times, flow.
- *Liver*: Quantitation of fibrosis and changes in tissue elasticity accompanying disease progression.
- Hyperpolarization or chemical shift imaging applications; applicable to lungs.
- *Limits* of resolution in image fusion: Optical, X-ray, PET/SPECT, and MR images.
- Regulatory: Validation of the platform(s) and novel imaging biomarkers.
- Cost: Appropriateness; always include a cost analysis.

A general view of what MRI can achieve in the small animal setting is seen in Fig. 11.1 which displays a set of serial slices (floor of the cranium up to the ventricles) of the mouse brain. This is a high-resolution high-field image set utilizing a 62×62 micron resolution in 150 micron slices. Typical small animal imaging, even in a 1.5 T machine, can achieve a useful resolution in a mouse and is a first-line approach in drug development imaging. Higher-field systems may be better suited to applications where sensitivity is limiting, but care must be taken to avoid neural stimulation when gradients are switched rapidly.

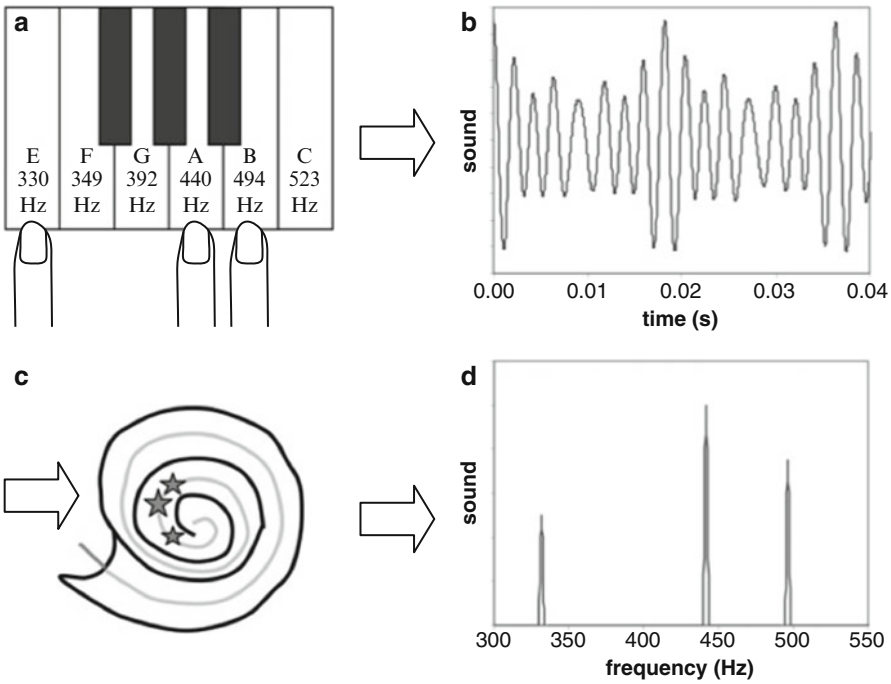

Fig. 11.2 Sound is produced as oscillations in air as a function of time and perceived as tones of specific frequencies. If three piano keys are struck (**a**), the vibration of the strings causes the air and thus the tympanic membrane of the ear to oscillate with time. If we measure these oscillations, they might look like the graph in panel (**b**). These sound waves produce an oscillation within the basilar membrane in the cochlea (**c**) where specific regions of the membrane (*indicated by stars*) respond maximally to the principal frequencies of the sound burst. The tonotopic mapping of the cochlea allows the brain to perceive the relative loudness of each specific frequency (or *piano key*), as shown in the spectrum (**d**). Both graphs (**b**) and (**d**) represent the sound produced by the piano and are related by the FT. The cochlea performs a natural FT. In an analogous way, the gradients of an MR scanner make tissues at different keys (locations) resonate at different frequencies, giving off a time signal measured by the receive coil that might look like the graph in panel (**b**). A computer, rather than a cochlea, performs the FT to reveal an image of the relative signal strength of each key (tissue location), analogous to the graph in (**d**). Reprinted from Paschal and Morris (2004). With permission

The physics of MR is complex and challenging, but the basic principle is simple: a population of hydrogen nuclei will behave like tiny magnets, each aligning with or against the static magnetic field B_0, and the whole having a small net magnetization vector precessing at the Larmor frequency around B_0. A perpendicular pulse of radiofrequency energy along the B_1 axis and at the same Larmor frequency causes the net magnetization vector to "tip" and reorient along B_1. After the B_1 pulse is turned off, the magnetization returns by T_1 and T_2 relaxation to the B_0 axis, emitting radiofrequency electromagnetic energy which allows a remote coil to sense the energy; based upon the induction field strength and the pulse sequence of the initiating radiofrequency, the exact position of the response can be mapped in what is termed K-space (Fig. 11.2).

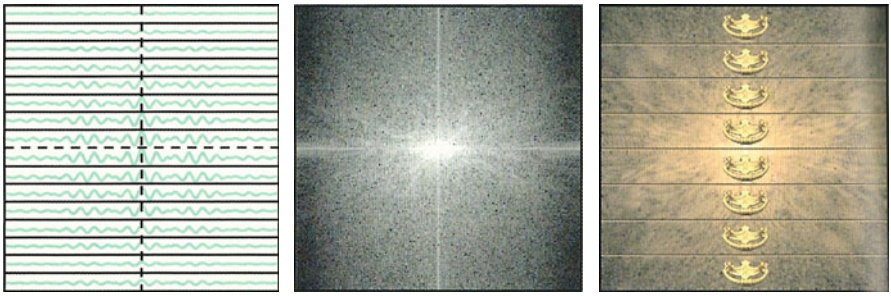

Fig. 11.3 A pictorial description of "K-space" for one slice of an image. The graphic shows a map of phase versus the frequency. That is, the graphic shows a spatial frequency domain where location of the signal within the subject is contained. Frequency is defined here in terms of phase change over distance (measured in radians). The units of K-space are radians per cm

MRI signals are similar to sound in that they can be presented in two equal ways, as either functions of time (t) or frequency (Hz or $1/t$). The reciprocal relationship between these variables is no accident and carries with it a great deal of physical and mathematical utility. If we strike a chord on a piano, several strings vibrate at a specific frequency. These frequencies mix to form a superposition of waves that we can pickup in a microphone or the tympanic membrane of our middle ear. The oscillations can then be decoded by the cochlea due to its frequency-specific mapping. Mathematically we can perform the same operation to recover the individual pure tone and amplitude of the keys in the chord.

In this fashion, MRI signals produce a superposition of all components in the RF-excited portion of the patient/animal which is then detected and digitized. The spatial information that is available in this signal has been encoded by the MRI scanner in such a way to fill a grid line (or K-line) in K-space. Each successive acquisition will fill another K-line such that we will fill our image K-space uniformly. Using a mathematical technique known as Fourier analysis, we can transform the signal into a number of weighted coefficients that will make up the intensities of our image. Thus we have used the Fourier transform to "transform" our K-space time-varying data to an image based on frequencies. MRI has a great deal of flexibility on how it fills in K-space and a great deal of image contrast, resolution, and clarity can occur due to the manner in which K-space is filled. The popular technologist training book, *MRI in Practice*, uses an interesting paradigm as a "chest of drawers" to describe the orthogonality of the phase versus frequency axes of K-space. In this manner, we can think of each drawer as being a rapidly scanned K-line and we sequentially acquire each "drawer of information" as an acquisition (Fig. 11.3).

The leftmost image in Fig. 11.3 shows the ordering and line information describing the K-space data of phase versus frequency. K-space itself is not the image; rather, it is an information package of an image. The "diagrammatic" representation highlights the acquisition order for a rectilinear MR K-space strategy. The actual data shown in Fig. 11.3b demonstrates the center-out character of K-space where the

low-frequency components of the image (contrast, total signal amplitude, etc.) are located around the K(0,0) point. Following Fourier transform (FT) computation in one or more directions, the "package" converts the K-space phase versus frequency into frequency amplitudes which is actual positional information.

Figure 11.4 is a demonstration of this positional transformation as it shows an image derived out of K-space order (Fig. 11.4a). By removing the center points of K-space (Fig. 11.4b), the resulting image consists of short-range or high-frequency edge transitions that show only line like image structures without any image contrast. Similarly, when transforming only the low-frequency components (Fig. 11.4c) results in a near-interpretable image based on contrast and large scale structures but at low spatial resolution.

A large number of methods or sequences have been developed to acquire MRI images and thus fill K-space most efficiently for the application and results desired. Simply by changing the K-space filling order from edge-to-edge sequentially, center-out, or center-in K-line ordering, it is possible to change the contrast of the image especially when changes in state to the imaging region are in progress (i.e., contrast agent washout). Table 11.2 includes some of the most common K-space filling orders in currently in clinical use. The major types, sequential rectilinear, EPI, and parallel imaging, account for a vast majority of the K-space ordering used. Some knowledge of these techniques will allow the reader to be more discerning about the strengths and weaknesses of each method when encountered in the literature.

11.2 Contrast Agents for Pharmacological Imaging

The field of MR imaging has greatly been improved, and indeed expanded, in capability with the introduction of contrast agents. Not unlike CT with X-ray contrast media such as the iodinated products, MRI has contrast-enhancing products. Unlike CT contrast agents which are electron dense and directly affect the X-ray absorption, MR contrast agents are typically not "seen" per se; rather, they affect the magnetic susceptibility and thus the tissue water imaging properties (not the media itself). Magnevist (formerly Schering AG, now Bayer) was approved for use by the FDA in 1988 and it revolutionized the kinds of imaging approaches one could take on then-typical systems with limited field strength and often stability and homogeneity issues too. Since that time there have been many other contrast media products introduced (Table 11.2). The products are termed "linear" or "macrocyclic" and "nonionic" and "ionic" to describe their chemistries; the macrocycles are supposedly more chemically stable than the linear variants, while nonionic agents in bolus form may be less perturbing to the heart, for example. These kinds of agents generally require a paramagnetic atom or ion: gadolinium (Gd), dysprosium (Dy), iron (Fe), and manganese (Mn), among others, have been employed for this purpose.

The Fe ion is, of course, intrinsic as a physiologic element predominantly in hemoglobin, myoglobin, and red blood cells. It is also very effective in what are

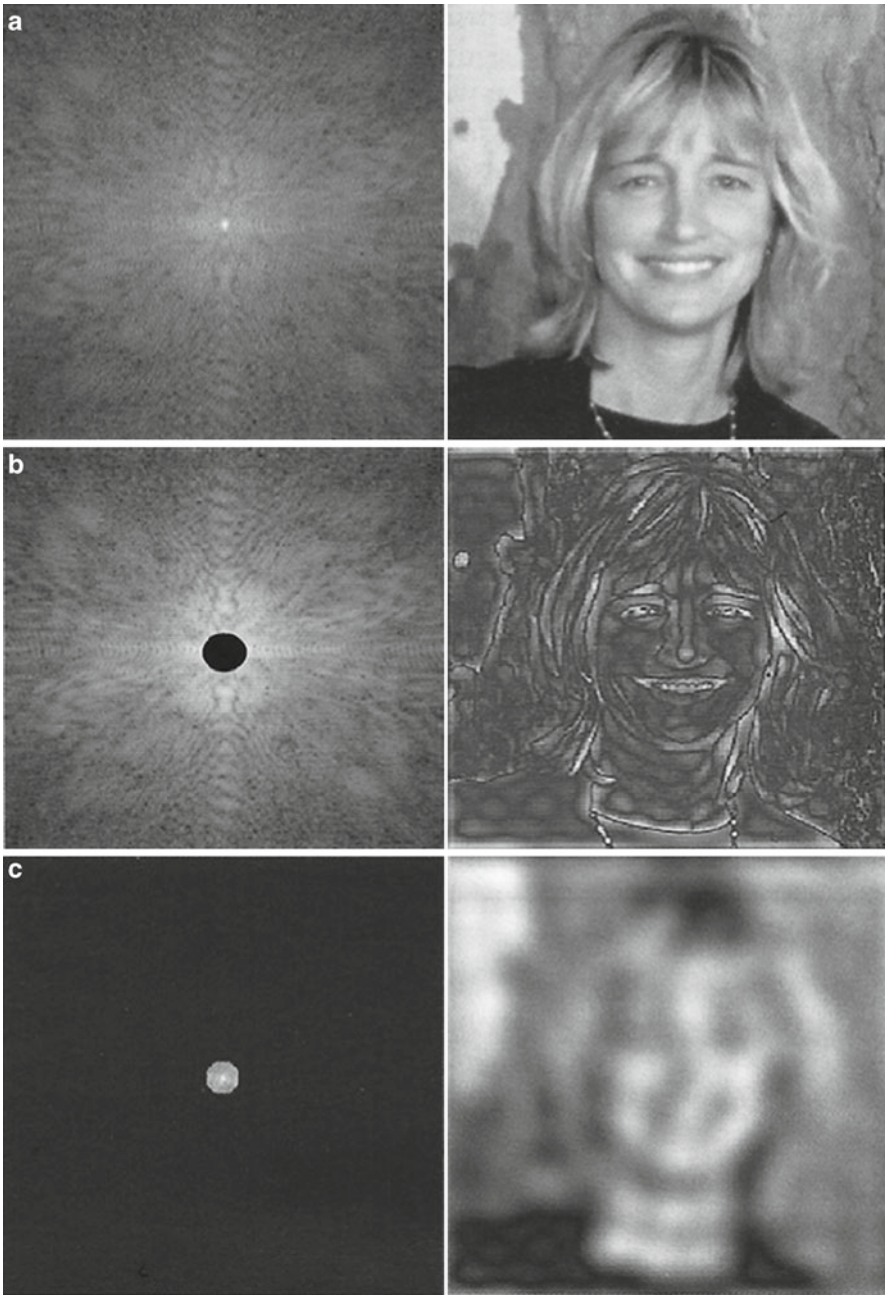

Fig. 11.4 A depiction of the spatial information contained in K-space. The entire K-space information is passed through a Fourier transform to which transforms frequency amplitude to frequency-domain (positional) space to create the image in where (**a**) is the entire K-space, (**b**) is everything but the center information (high resolution but poor content), and (**c**) is the center information only (poor resolution with high content). Magnetic field gradients spatially locate signals according to their frequency and converts to amplitude (positional intensity). From: Westbrook et al. (2011); with permission

Table 11.2 Clinically relevant K-space filling strategies. This table summarizes the some common methods for filling K-space, organized according to trajectory

Trajectory	Variants	Rationale	Utility
Non-EPI rectilinear	Sequential	Every k_y step is acquired as a individual readout ordered from top to bottom of K-space	All standard imaging sequences where contrast is constant over excitations (steady state imaging)
	Centric	Every k_y step is acquired as a individual readout starting with the center line ($k_y = 0$) and alternating ($+k_y$ and $-k_y$) on subsequent excitations	Used for applications where initial transient contrast dominate the image (i.e., a preparatory RF stage or contrast injection—non-steady state)
	Reverse centric	Every ky step acquired in a separate readout, starting with the outer lines of K-space ($k_y = +k_{y,\,maximum}$ and $-k_{y,\,maximum}$) and working inward from either edge in successive excitations	The final relative contrast dominates the image contrast, typically used after a preparatory pulse such as inversion (non-steady-state imaging)
	View-sharing	Incomplete sets of k_y lines acquired for different cine phase images. Share k_y lines between temporally adjacent readouts to fill K-space for each cine phase image	Cine applications use short scan times and high temporal resolution with good spatial resolution. A consequence is temporal blurring (heart and abdominal scans)
	Partial or half Fourier	More than have the k_y lines are acquired and using K-space symmetry estimate the missing data	Rapid scan requirements such as cardiac, interventional or dynamic contrast applications. Results in a reduction of ~2 in scan time at the cost of 1/sqrt(2) reduction in signal-to-noise ratio
	Zero filling or Fourier interpolation	Central k_y lines are acquired (minimally half the desired matrix size) and substitute zero for the missing data points. "Zero filling" in K-space is equivalent to a perfect interpolation of a low resolution image to a higher resolution image without linear or polynomial limitations	Rapid scan requirements such as cardiac, interventional or dynamic contrast applications also. Results in a reduction of N in scan time at the cost of 1/sqrt(N) reduction in signal-to-noise ratio

(continued)

Table 11.2 (continued)

Trajectory	Variants	Rationale	Utility
EPI—echo planar imaging	Single shot—blipped	Traverse all of K-space, starting in one corner, sweeping across the k_x axis for a given k_y value, turning ("blipping" or formally "boustrophedon") to the adjacent k_y line and sweeping back across the readout axis. Following the boustrophedon to the next k_y line and so forth until K-space is completed	Very high speed applications such as functional MRI (fMRI), stroke (DWI) or diffusion tensor neuroimaging (DTI). Distortions and T_2*-dependent signal loss limit the acquisition of a high-resolution image
	Multi-shot—blipped	Increase the granularity of K-space travel, beginning at one edge acquiring a readout turning the boustrophedon to the next non-adjacent k_y line and acquiring the readout, and so forth. Using a fraction of K-space equal to $1/N_{shots}$). N_{shots} excitations used to complete the image	Not as fast as single-shot EPI. Used for rapid applications (fMRI, DTI) for higher resolution images. Less distortion and higher signal-to-noise ratio than single-shot EPI
Parallel imaging	GRAPPA	Uses specific receiver coil geometries create additional K-space data without added scans. Auto-calibrates using central K-space lines	Used for reduction in imaging time where a reduction in image SNR is offset by high efficiency receiver coils
	SENSE	Receiver coil sensitivity maps are used to compute additional k_y lines in K-space from unders-ampled (factor of 2–8) data	Rapid scanning applications that use the high efficiency receiver coil arrays to reduced SNR losses due to scan time reduction

termed SPIO (super paramagnetic iron oxide) applications. SPIO magnetic resonance imaging can be used in liver pathologies, i.e., nonalcoholic fatty liver disease, as a way to evaluate Kupffer cell phagocytic function. Iron oxide (as SPIOs) can be also used in cell labeling and thus tracking cells and their homing capacity. With typical pulse sequences and at the relatively high field strengths common in small animal imaging, iron is usually considered to be a specific T_2 imaging agent meaning that its principal effect is to shorten the tissue T_2 causing a signal "drop out" (reduction) rather than giving a signal enhancement such as might be expected with a T_1 contrast agent.

In the ionic form, manganese (Mn), gadolinium (Gd) and dysprosium (Dy) from the lanthanide series exert a dramatic effect on the relaxation properties of water. This effect results from unpaired electrons in the *d* or *f* atomic shells, which give rise to a strong magnetic moment. Other elemental examples include Cr^{3+} (3 unpaired electrons), Fe^{3+} (5 unpaired), Ni^{2+} (2 unpaired), Cu^{2+} (1 unpaired, with dipole contributions from the *d* shell), Eu^{3+} (6 unpaired), Gd^{3+} (7 unpaired), and Dy^{3+} (5 unpaired, with contributions from the *f* shell). Although the properties of each ion govern its utility in imaging, the strength of an ion's effect on contrast will depend upon the strength of the magnetic moment.

The effect of these ions on the excited ^1H nuclei (which comprise the MRI signal) depends on multiple components. First, the dipoles of the ions may interact with nuclear ^1H dipole, which in turn stimulates spin–flip transitions and accelerates T_1 relaxation of ^1H. The strength of this interaction depends on the approach distance between ^1H and the ion. If the ion is part of a larger molecule (e.g., deoxyHb), large distance leads to a small interaction. The effect magnitude of the dipole–dipole interaction is also modulated by the correlation time which determines the duration of the coupling between ^1H and ionic dipole. To increase coupling, the rotational rate of the ion or chelating molecule should be similar to the excitation frequency of ^1H. If the ion is not chelated, it will have a wide range of rotational velocities compared to the excitation frequency of ^1H. In this case, the dipole–dipole interaction is weaker. For suitable rotational rates, the correlation time will depend on the electron spin relaxation time of the agent, where slower electronic relaxation results in greater coupling of the dipoles. Ultimately, relaxation rates should be comparable to the ^1H Larmor frequency for an agent to be effective at increasing T_1 relaxation. Electron spin relaxation times for ionic Mn and Gd are ~10^{-8} to 10^{-10} s and appropriate for the range of Larmor precessional frequencies in clinical scanners. Larmor precession refers to the precession of the magnetic moments of electrons, atomic nuclei, and atoms about an external magnetic field. Those effects which lead to spin–flip transitions also result in randomization of ^1H phase after de-excitation and result in increased local T_2 relaxation. Finally, the presence of the paramagnetic dipoles around less mobile ^1H nuclei (e.g., water in the hydration shells of tissue macromolecules) alters the local precessional frequency, which further increases T_2 relaxation.

Consideration of all these effects together determines the ratio of T_1 and T_2 relaxation rates for a given concentration. Like other forms of emission spectroscopy, these characteristic relaxation processes return the nuclear magnetization back to

the equilibrium distribution after being excited. Ions with longer spin relaxation time (e.g., Mn^{2+}, Gd^{3+}) tend to stimulate spin–flip transitions effectively and are useful for enhancing contrast positively on T_1-weighted images. At higher concentrations, they are also useful for increasing T_2 relaxation resulting in local loss of signal in the image. Increased signal is particularly useful because it usually has a higher dynamic range and can be quantified more accurately than a loss of signal. Typically, paramagnetic agents, such as chelated Gd, increase T_1 and T_2 relaxation at the same rate per mM. Since this rate is the same, the change of T_1 relaxation per mM is larger by proportion than the change in T_2 relaxation. On the other hand, ions with shorter spin relaxation times, such as dysprosium (Dy^{3+}), do not stimulate spin–flip transitions readily. These ions function primarily to vary the local Larmor frequency (they are said to act as "chemical shift agents") and therefore to decrease the intensity on T_2-weighted images which are formed from protons precessing at or very close to the original Larmor frequency. While Mn^{2+} may not have as strong of a magnetic moment as other agents such as Gd^{3+}, the T_2 relaxation rate (R_2) of water containing Mn^{2+} ions at 1.5 T grows at 10× the rate per mM as compared to the T_1 relaxation rate (R_1). This makes Mn^{2+} a valuable agent for both T_2 and T_1 imaging, the effect depending on the field strength and the local concentration of agent in the tissue.

Another avenue to increase the T_1 relaxivity is to chelate the paramagnetic ions to a larger molecule so as to decrease their rotational velocity and increase the rotational correlation time. An added benefit of using a chelate is that for less chemically reactive but toxic metals, such as Gd, the chelated complex is excreted from the body within a short timescale (approximately a few hours). This greatly decreases potential toxic side effects, although in some patients with altered kidney function gadolinium contrast agents have been associated with severe toxicities causing the FDA to require a black-box warning to be included in the label (see Sect. 11.2.1. Nephrogenic Syndrome). Examples of chelates that have been used include Gd-DTPA, Gd-DPDT, Gd-DOTA, and other macromolecules such as MnDPDP, Cr-EDTA, and Dy-EDTA. Nonionic molecules have also been utilized to prevent the release of the ion and to decrease the rotational velocity.

Manganese dipyridoxyl diphosphate (MnDPDP) is approved as an i.v. contrast agent for MR imaging of the liver. MnDPDP is a chelate consisting of the organic ligand dipyridoxyl diphosphate (DPDP) and Mn^{2+}. Following i.v. injection, MnDPDP is metabolized by a process involving dephosphorylation of MnDPDP to MnPLED (manganese dipyridoxyl ethylamine) and exchange of Mn^{2+} for Zn^{2+} (Toft et al. 1997) with the consequent release of manganese ions. In humans the rate of total manganese plasma clearance is multiphasic (Toft et al. 1997). The initial clearance half-life lasts for less than 20 min, with the longer terminal elimination phase occurring between 5 and 11 h. Following i.v. injection of MnDPDP, the released manganese accumulates in the liver, bile, pancreas, kidneys, and cardiac muscle (Hustvedt et al. 1997). Following oral intake the manganese accumulation occurs only in the liver and bile (Thomsen et al. 2005). Due to its T_1 relaxation effect, the released Mn^{2+} ions act as an MR contrast agent (Cory et al. 1987; Mendonca-Dias et al. 1983) which allows MnDPDP to be used as an MR contrast agent.

11.2.1 Gadolinium Nephrogenic Syndrome

Gadolinium ions have known toxicities and as such any use of Gd requires the chemistry of the contrast agent keep the ion "caged" in chelation to maintain safety. The safety issue for gadolinium is known as nephrogenic syndrome (fibrosis) (Kanal 2008). It is primarily a skin phenomenon but can affect internal organs as well. Originally termed nephrogenic fibrosing dermopathy (NFD) due to its proclivity for the skin, it was eventually found to actually include systemic tissues and organs. Gadolinium-based MR contrast agents (GBMCAs) which have received FDA approval include, for example, Omniscan™ (gadodiamide) which is the one agent that accounts for most of the nephrogenic syndrome reports. There are two others that contribute to the total incident count and they are Magnavist™ (gadopentetate) and Optimark™ (gadoversetamide). It is apparent that most of the patients developing this syndrome are also in end stage renal disease, are >60 years of age and have a history of diabetes or a history of severe hepatic disease/liver transplant or pending liver transplant. Present recommendations from the ACR MR safety committee can be found at http://www.acr.org/mr_safety (Kanal et al. 2013). An excellent review of the safety of contrast agents in MR is provided by Kirchin and Runge (2008).

11.3 MRI and Functional MRI (fMRI) Applications

MRI and fMRI have advanced their footprint in the drug development laboratory with increasing improvements in system adaptations to small animals and novel imaging pulse sequences which have expanded both anatomical and functional capabilities. Functional MR imaging (fMRI) is an imaging technique that can evaluate blood flow when at rest and following stimulation. It is particularly useful in the brain because of the well-defined and largely symmetric anatomy and the tight anatomic and physiological relationship between neural and vascular tissues, but it has been applied to other tissues. Two or more sets of images collected under different conditions (with and without some stimulus, e.g.) can be related mathematically and can be statistically correlated with each other to reveal the areas showing changes as a result of the stimulus, for example, the altered blood flow patterns in regions of the brain performing mental activation tasks. This methodology has been extended to brain studies where drugs (rather than physical or mental stimuli) can alter the activity of regional centers to show blood flow changes in the affected areas of the cerebral cortex. In the early days of fMRI, the change in flow was mostly seen using contrast agents but now the blood itself, and its intrinsic sensitivity to MR fields (oxyhemoglobin is diamagnetic vs. deoxyhemoglobin which is paramagnetic) allows one to image blood flow without contrast. Venous blood contains an almost equal mix of oxy and deoxyhemoglobin. With exercise (change in oxygenation) more oxygen is needed and thus the oxy component is extracted from the capillaries changing the "delta." Paramagnetic deoxyhemoglobin creates an inhomogeneous magnetic field in the immediate vicinity in the brain and this in turn increases the T_2* decay and attenuates the MR signal. The MR signal intensity change is called the BOLD or "blood-oxygen-level-dependent" effect.

The notion that MRI could be sensitive enough to measure brain activity, in addition to brain anatomy, is only about 20–25 years old. An observation was made that when neural activity was seen to increase in a particular area of the brain, the area had a measurable MR signal that also increased by a small amount. Although this effect had a magnitude change of close to 1 %, it was seen to be consistent and measurable with high accuracy and is now a major basis as to why fMRI has taken off as a very useful MR tool in neurologic diseases, chemical injuries, blood–brain barrier breaches, and even in psychopharmacology in cognitive neuroscience. The applications of fMRI in translational medicine and clinical practice are becoming an important tool to measure plasticity of neural recovery (surgery and trauma) and maintenance of brain function under stresses and disease.

In its simplest form, fMRI places a subject under conditions where the subject alternates between periods of doing a particular task and placing himself back into a stable (cognitively speaking) control state. This could, for example, be structured as 30 s blocks looking at a visual stimulus alternating with 30 s blocks with eyes closed. The fMRI data is analyzed to identify brain areas in which the MR signal has a matching pattern of changes and these areas are taken to be activated by the stimulus (in this example, the visual cortex at the back of the head).

It is not because the MR signal is directly sensitive to the neural activity. Instead, the MR signal change is an indirect effect related to the changes in blood flow that follow the changes in neural activity. The picture of what happens is somewhat subtle and depends on two effects. The first effect is that oxygen-rich blood and oxygen-poor blood have different magnetic properties related to the hemoglobin that binds oxygen in blood. This has a small effect on the MR signal, so that if the blood is more oxygenated, the signal is slightly stronger. The second effect relates to an unexpected physiological phenomenon. For reasons that we still do not fully understand, neural activity triggers a much larger change in *blood flow* rather than in *oxygen metabolism*, and this leads to the blood being more oxygenated when neural activity increases. This somewhat paradoxical *blood-oxygen-level-dependent* (BOLD) effect is the basis for fMRI (Fig. 11.5).

The orderly and sequential accretion of cognitive milestones in the typically developing child constitutes a most fascinating facet of childhood development. The establishment and use of cognitive developmental screening instruments such as the Denver Developmental Screening Test and the Wechsler Intelligence Scale for Children (WISC-R[1]) reflect the normalized and chronologic pattern of cognitive development documented in children. Recent advances in neurobiology have provided new understanding of cellular events that underlie neuronal function in the central nervous system. While this critical information sheds light upon function of the brain at a microanatomic level, it sheds little light upon the ways in which the neural tissue of the brain functions as an interrelated network of subsystems to produce human behavior and cognition.

[1] Refer to Wechsler Intelligence Scale for Children http://www.pearsonassessments.com/HAIWEB/Cultures/en-us/Productdetail.htm?Pid=015-8979-044.

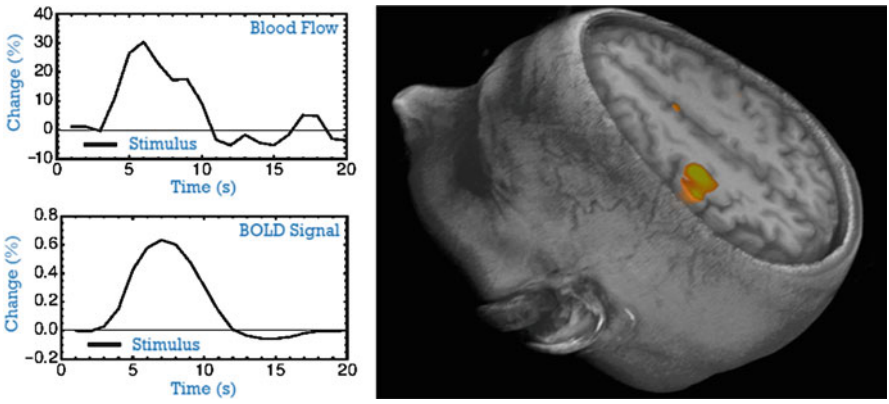

Fig. 11.5 fMRI is a way to describe and image changes in localized blood oxygenation. Depicted in the figure is a theoretical location in the brain where blood flow is measured and the concomitant BOLD signal parallels the time course and relative area and modulation profile. UCSD, Center for Functional MRI, *Why is the MR Signal Sensitive to Changes in Brain Activity?* http://fmri.ucsd.edu/Research/whatisfmri.html. *Left image*: reproduced from Buxton (2010), based on data from Miller et al. (2001); *Right image*: reproduced from Buxton (2002)

11.3.1 Small Animal and Pediatric Applications of fMRI

One of the major uses of fMRI is in early childhood development in the assessment of disease, cognitive impairments, and functional deficits. This is even true in the fetal subject where certain regions of the brain can be assessed for blood flow preterm. Table 11.3 gives a time line of major development events and anatomical information can be collected via MR imaging and the cofunctional component may also be explored using fMRI. In fetal imaging blood flow changes can be monitored using metronomic sounds as a form of stimuli. The use of anesthetics to prevent motion during a scan may be necessary with small children but it is common in small animal imaging; care must be taken that the anesthesia does not unduly perturb the physiology being studied (there are effects on cerebral blood flow and blood glucose levels to consider, e.g.). Again, the reader is encouraged to seek further information on small animal imaging with MRI in the textbooks of Westbrook et al. (2011) and Gavin and Bagley (2009).

The regional blood flow in young children can be measured using task-oriented tests (reading, writing, physical movement) or passive testing such as auditory stimuli, tactile sensory stimuli, smells, and perturbations in light exposure. Each of these activities can change blood flow associated with the brain region of interest. Rivkin provides some examples in these tests in Fig. 11.6. fMRI has pediatric challenges but it also has issues of reproducibility in the aged and in certain diseases such as dementia where comprehension is required (D'Esposito et al. 2003).

Table 11.4 on the pediatric neuroanatomy development schedule and Fig. 11.7 showing pediatric brain blood flow using fMRI are presented as examples of the complexity involved in pediatric MR imaging. Age dependent brain anatomic

Table 11.3 Major Gd and Mn contrast agents and their physical attributes for imaging[a, b]

Characteristic	Magnevist	ProHance	Omniscan	MultiHance	Gadovist	OptiMARK	TeslaScan
Type	Linear, ionic	Cyclic, nonionic	Linear, nonionic	Linear, ionic	Cyclic, nonionic	Linear, nonionic	Complex cage see figure "a" below[c]
Paramagnetic ion	Gd	Gd	Gd	Gd	Gd	Gd	Mn; MnDPDP
Metal chelate (mg/mL)	469	279	287	334	605	331	2.75
Dosage concentration	0.5 mol/L	0.5 mol/L	0.5 mol/L	0.5 mol/L	1.0 mol/L	0.5 mol/L	5 μmol/kg
Osmolality (Osm/kg)	1.96	0.63	0.65	1.97	1.6	1.11	2.98
Viscosity (mPa s @ 37 °C)	2.9	1.3	1.4	5.3	4.96	2.0.	Not available
T_1 relaxivity L/mmol s @ 0.47 T in plasma	4.9	4.6	4.8	9.7	5.6	Not available	r1 = 2.3, r2 = 4.0 (@ B_0 = 1.0 T)

[a]Table adapted from Kanal (2008)

[b]Note: Fe paramagnetic products include SPIO (superparamagnetic ion oxide; particles) for cell labeling and other applications

[c]Figure "a": The MnDPDP structure. For Gadolinium contrast agent cage structures the reader is referred to Faulkner (2008):

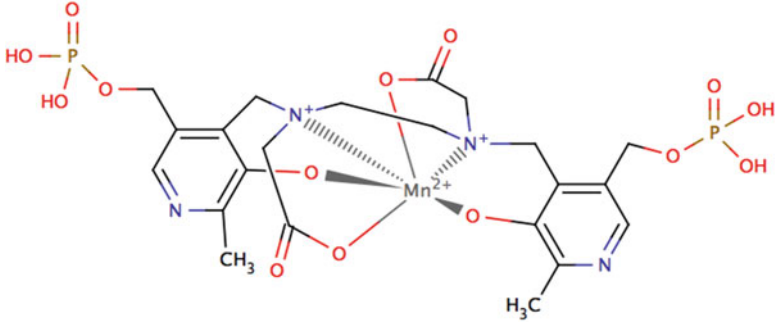

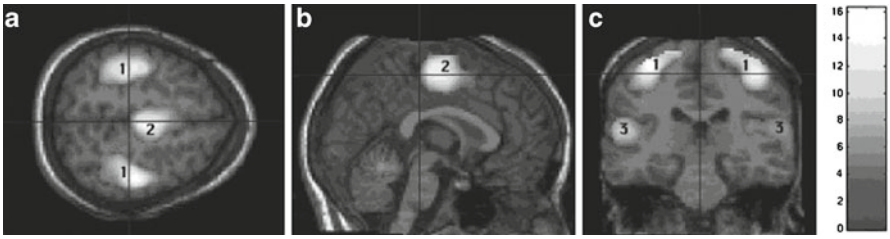

Fig. 11.6 fMRI imaging in pediatric (nonverbal task) conditions. Group analysis of data obtained during fMRI study of four 9- to 10-year-old normal volunteer children. The children were instructed to perform bimanual alternating finger tapping to match the rhythm of a metronome beat delivered to them simultaneously by earphones. The statistical color map of regional activation is rendered upon the high-resolution T_1W image of one of the subjects. The axial image (**a**) demonstrates activation of primary motor cortex (areas marked by 1) and supplementary motor cortex (area marked by 2). The sagittal image (**b**) provides a medial view of supplementary motor cortex (area marked by 2). The coronal image in (**c**) reveals the same regions of primary motor cortex (areas marked by 1) activation found in (**a**). In addition, the superior temporal gyri (areas marked by 3) reveal significant activation indicative of their role in hearing the metronome beat (from: Rivkin 2000). The nonverbal task approach is applicable to small animal studies

Table 11.4 Major events in human brain development and peak times of occurrence[a]

Major development event	Peak time of occurrence
Primary neurulation	3–4 weeks' gestation
Prosencephalic development	2–3 months' gestation
Neuronal proliferation	3–4 months' gestation
Neuronal migration	3–5 months' gestation
Apoptosis	6 months' gestation-1 month postnatal
Synaptogenesis and organization	5 months gestation-years postnatal
Myelination	Birth-years postnatal

[a]Adapted from Rivkin (2000)

changes in newborns can confound image interpretation of blood flow patterns. Brain tissue arterial input and venous drain (i.e., flowing blood) is what is imaged in fMR. As blood passes through a selected brain slice an RF pulse is applied to the slice and the blood within the slice experiences a phase change which allows for localized angiographic evaluation.

In brain cancer, fMRI has a practical application (Young and Knopp 2007). fMRI provides activation maps of the brain cortex that reflect hemodynamic activity related to neuronal activity. As discussed preciously, the BOLD signal of local tissue oxygenation measures the magnetic property changes of hemoglobin as blood traverses through a vascular network as an intrinsic contrast agent. The effect of oxygenation of a brain voxel element is an increased diamagnetic oxyhemoglobin and decreased paramagnetic deoxyhemoglobin. Measurements within the brain locations for speech, language, comprehension, memory, and motor skills which may be altered by tumor invasion can be measured and efficacy of treatment assessed. Preoperative fMRI can help the physician (or nonclinical investigator) to better determine the BOLD valuations of the tumor margins, control regions of the brain, supplemental cortex, and globally the bilateral hemispheres. Increased tumor

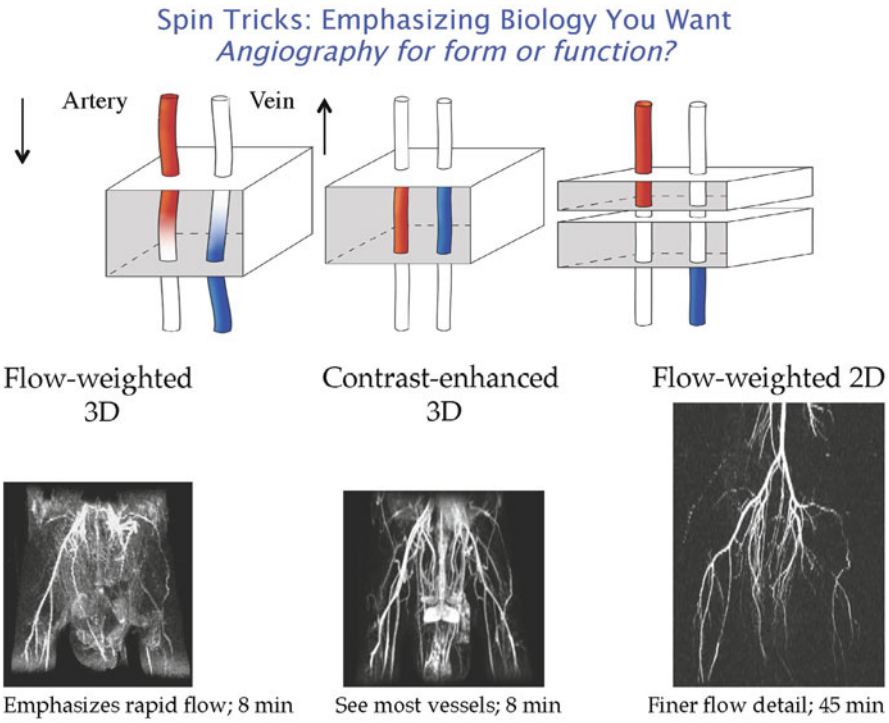

Fig. 11.7 Depiction of flow, where magnetic transference occurs within an MR image slice, which may be mapped to show relative change through a targeted vessel. Courtesy of Simon Williams, Genentech, So. San Francisco

vascularity provides a measure of the grade of the tumor. The interpretation of the BOLD signal, however, requires some caution toward use as a clinical or translational tool for assessing drug-induced differences in fMRI images (Logothetis and Wandell 2004; Matthews et al. 2006)

Ferrari et al. (2012) provide an excellent review of an experimental protocol for rats and mice to evaluating pharmacologic fMRI changes (phMRI, *ph*armacologic or *ph*ysiologic MRI). They discuss the role of anesthetics (isoflurane and halothane) and chemical use, animals and the constraints on the animal models, animal preparation, tracheotomy (for controlled ventilation), vessel cannulations appropriate for the MR contrast agent administration and blood gas determinations in the MR environment, arterial gas measurements, relative cerebral volume (rCBV), use of a 4.7 Tesla system T_2-weighted anatomical images using RARE sequence (RARE; rapid acquisition with relaxation enhancement) as well as conventional spin-echo sequences, and use of the blood pool contrast agent Endorem® (Guerbet, France). The methods they report are limited in that this is not set up for chronic measurements. However it has excellent applications in the study of neuroscience and psychopharmacology. Figure 11.8 depicts physiologic (or pharmacologic) phMRI images (Becerra et al. 2013).

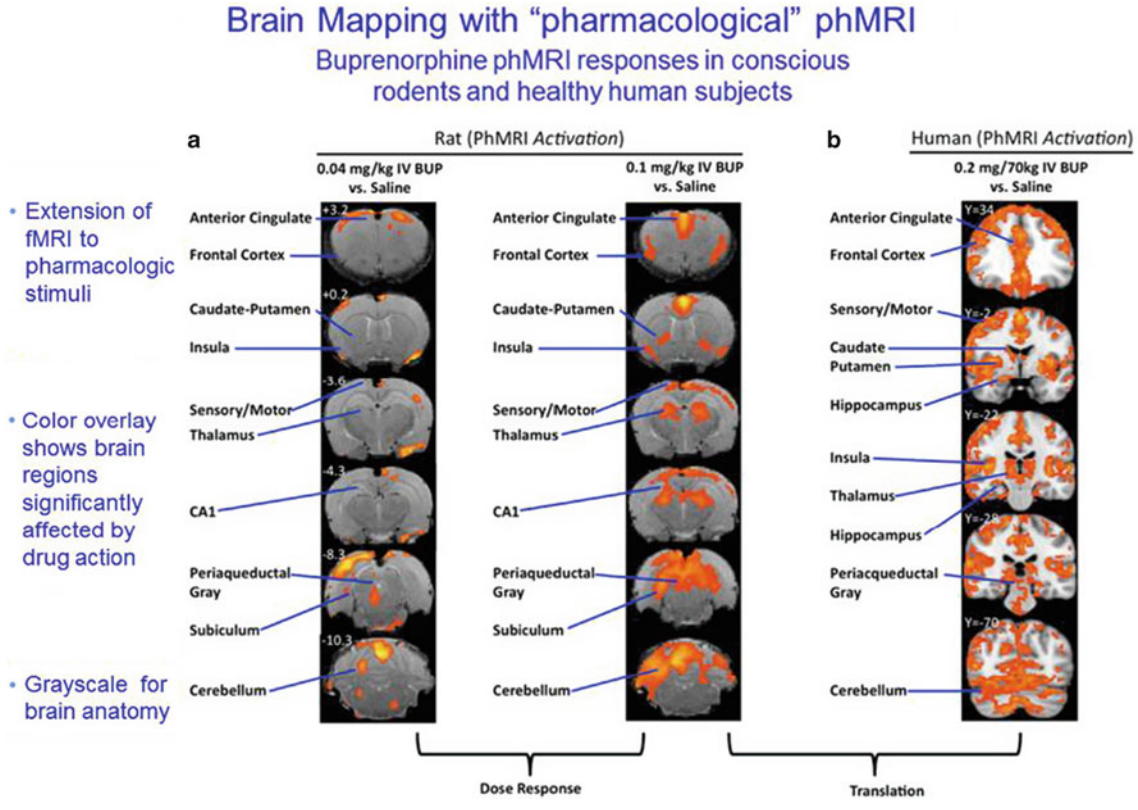

Fig. 11.8 Physiologic/pharmacologic MRI. phMRI for brain mapping of drug intervention in the rat (**a**) and in the human (**b**) conscious brain. Images depict both rodent and human response maps of activation by buprenorphine (BUP). From: Becerra et al. (2013); with permission

11.3.2 MR Imaging and Psychopharmacology

Yurgelun-Todd et al. (2005) describe in their paper a study of fMRI imaging in schizophrenic patients during word production and the pharmacologic effects of D-cycloserine (D-CS). D-CS, a partial agonist at the glycine recognition site of the n-methyl D-aspartate (NMDA) receptor, can improve primary negative symptoms in schizophrenics. Rats administered the drug MK-801, an NMDA antagonist, have been shown to have a deficit in spatial memory which can be reversed by D-CS. D-CS thus serves as a neuroleptic for the structural and functional abnormalities in the frontal and temporal cortex of schizophrenics. The effect of D-CS in cognition is less well understood. Previous work using verbal cognitive challenge testing an fMRI in controls and schizophrenics showed control subjects had greater activation of the left dorsolateral prefrontal cortex region relative to the schizophrenics. Schizophrenics exhibit hypo-frontality and neuroleptic therapy increases activation in the left temporal lobes relative to nonpsychiatric controls. Using fMRI they were able to show that D-CS plus neuroleptics augmented temporal lobe activation in schizophrenic patients relative to neuroleptics alone. They were also able to surmise that enhanced temporal lobe activation was negatively associated with a reduction in negative symptoms. Word fluency was effectively augmented in subjects administered D-CS, and the fMRI results demonstrated that the temporal lobe activation directly correlated with the temporal drug induced change in blood flow which characterized the temporal lobe activation.

Roe and Chen (2008) provide a very good paper on high-resolution fMRI maps of cortical activation in nonhuman primates (NHP), a very prominent model in testing brain changes due to drug activity, i.e., psychopharmacology. They were addressing a method to map high spatial (submillimeter) resolution of cortical activity in the NHP brain. They note that other methods have been able to report at this level such as with optical imaging which has contributed in confocal microscopy in brain layers at the mm-plus dimension. Can fMRI also map the NHP brain at such resolution? Their hypothesis was "yes." They studied the ability of BOLD fMRI to measure submillimeter resolution of the NHP cortex. Digital (hand, digit 3, D3, e.g.) stimulation leads to focal activation at the cortical location of D3 activation/stimulation and also stimulation of D4 was mapped to the D4 location in the cortex—using optical probes. The stimulation of D3 and D4 should lead to two activation spots, but what was observed was only *one* central location stimulation suggesting an illusionary perception. They observed that stimulation of the skin is not only a *surface topography* map but also a *perception* map. The brain serves as an integrator of signals for general "perception." This was observed using optical probes and set the standard resolution required to test their hypothesis of obtaining similar information using fMRI. Consistent with the optical experiments, simultaneous stimulation of D3 and D4 in squirrel monkeys produced a single fMRI central focal cortical activation with 0.5 mm resolution image of the central stimulation spot. This kind of resolution has potentially profound implications in measuring psychopharmacologic drug interventions in the NHP model.

Mitterschiffthaler et al. (2006) discuss the utility of fMRI in psychiatry. The utility of psychiatric assessments in translational species remains in question but certainly changes in their physiologic parameters (as phMRI; refer to Fig. 11.8) by drug induced physiologic actions can be imaged and quantified in the non-clinical setting.

11.3.3 The Apparent Diffusion Coefficient (ADC) and Stroke

As most clinical and preclinical MRI is based on looking at the hydrogen nuclei of large concentration compounds such as water and fat, it is possible to sensitize the image to the structure below the level of the image resolution. One of the strengths of MRI is the ability to make relatively small changes in pulse sequence to be sensitive to certain physical effects. In this manner, we can make the sequence diffusion-weighted image (DWI). DWI is can probe the integrity of cell membranes, the changes in microvascularity in tumors, and changes due to osmotic shock as in strokes or thrombosis. Diffusion sensitivity is produced by adding strong gradient pulses that encode nonlinear movement due to Brownian motion of water molecules traversing the local environment. The diffusion length scale can probe dimensions as small as a micron or as long as 10 s of microns by varying the length, amplitude, and spacing of the diffusion gradients. Using this flexibility other applications of diffusion sensitized MRI can be detecting and following neuronal fiber tracts in the brain, spine, or major nerves. In like manner, diffusion-based methods can be used to track muscle fibers in skeletal and cardiac muscle. All of this done without any external contrast compound needed to be added. The basic diffusion-weighted image (DWI) technique, the Stejskal–Tanner sequence, uses a pair of high-amplitude gradient pulses in a spin-echo sequence with increasing amplitude,

$$I = I_0 \times \exp\left(-bD\right),$$

where $b = f(G, \delta, \Delta)$ and where G = gradient amplitude, δ = gradient spacing, Δ = gradient duration.

The signal, I, is reduced in amplitude from I_0 based on the amount of diffusive motion the water molecules undergo. In this technique, any motion produces a reduction in signal amplitude, I. Thus, it is possible to encode motion such as perfusion or in some limited case flow as a complicating effect. This apparent diffusion coefficient (ADC) yields a method to probe the microstructural integrity of tissue at a cellular level (Moseley et al. 2009). The ADC map can be obtained as a slope of a series of diffusion-weighted images with changing gradient strength (i.e., images collected at $b = 0$ s/mm^2), then, for example, $b = 250$, then $b = 500$, then $b = 700$, then $b = 1000$ s/mm^2, and then the natural log of the ratio of each image to the first image ($b = 0$) as log[Image "$b = X_o$"/Image "$b = 0$")] is plotted versus "b" to obtain the decrement in regional intensity with increasing gradient strength (Fig. 11.9). In stroke, the apparent diffusion is measurably slower (thus relative hyperintensity is retained in the infarcted area in the diffusion image) compared to normal brain areas by as

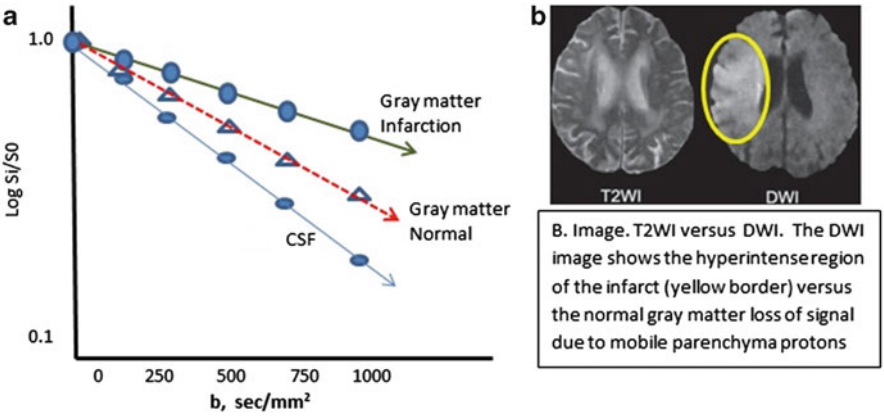

Fig. 11.9 The ADC profile (cm^2/s, or m^2/s). (**a**) *Plot*: An ADC map is obtained from a series of DW images with increasing *b* value (s/mm^2) here plotted as a series of regional area ratio values from $b = 0–1{,}000$. The ADC is the slope of the profile. Gray matter has a slope is less than the CSF (cerebrospinal fluid) and is commonly 1×10^{-5} cm^2/s, where the average displacement along one direction in the image is 8–9 μm observed over a 30–50 ms period. ADC regional decreases are highly correlated with areas of infarction (more mobile extracellular water protons). (**b**) *Image*: T_2WI versus DWI where the DWI shows the ADC hyperintense region of an ischemic stroke (*yellow circle*) (From: Neil (2008), with permission)

much as 30–60 % decreases in the slope (a flattening of the slope) versus normal. Figure 11.9 depicts an infarcted region which remains hyperintense in a DW image versus that same slice imaged as a T_2-weighted image.

In the case of stroke, cerebral blood flow is compromised from the normal 12–20 mL/110 g/min to usually <12 or, at later time points, the region may be affected by increased flow, i.e., "luxury" perfusion, a condition called reactive hyperemia, where CBF is greater than 20 mL/110 g/min. Changes in CBF that are less than 12 will result in a hyperintense region of the DWI image (as seen in Fig. 11.9) which is a consequence of a decline in the apparent diffusion coefficient of water in passing through the brain parenchyma. In the chronic stroke brain environment (<12 mL/110 g/min), the ADC is elevated due to extracellular water content and low diffusibility.

In a trial conducted by Schlaug et al. 1997), they evaluated the relative ADC (rADC; a useful measure in preclinical studies as well), a ratio of lesions to control brain ROIs; they found that in stroke there are two phases for the rADC. That is, the rADC is reduced and lasts about 96 h staying at about 50 % of normal from the time of stroke onset. Then after 96 h an increasing trend in the rADC is observed from 50 % of normal to normal and then to elevation of rADC at times >7 days in excess of 200 % of normal. The persistent reduction in rADC in the first 4 h is suggested to indicate progressive cytotoxic edema rather than extracellular edema and cell lysis. Such an observation can thus allow investigations of rADC in test animal models with induced cerebral stroke (e.g., reperfusion injury following middle cerebral artery balloon occlusion rat models; Yang and Betz 1994).

Changes to the Fickian Diffusion model (Gaussian intensity decay) can be described using other DWI methods. One of the simplest methods is termed "diffusion kurtosis imaging" (DKI) where the deviations from Gaussian signal decay are mapped out using a kurtosis term to the normal (single mode) distribution (Jensen et al. 2005). This method purports to detect additional changes to the diffusion image which are masked by the ST model. A number of papers in recent years have applied this methodology to studies in neurology and oncology as a more sensitive detection for disease processes.

11.3.4 The ADC Applied to Conditions in Oncology

The reader is again referred to the Oncology chapter of this volume (Chap. 7) for a view of imaging platforms used in oncology and where the MR platform is described. MRI can be quite flexible in describing the tissue heterogeneity, vascularity, and microstructural changes found in tumor environments. Standard characterizations such as tumor perfusion, vascular bed integrity, and hypoxia can be measured via MRI based on water motion as tracked via diffusion or perfusion. Here we will specifically address the ADC and tumor blood flow/perfusion (and indirectly angiogenesis and blood volume). Krupnick et al. (2012) describe MRI protocols for the study of mouse lung tumors and these kinds of studies may be very valuable in the assessment of new chemical entities that target lung cancer in vivo. Indeed, their models are also quite relevant to the study of other lung pathologies including radiation injury which may include normal and lung cancer tissue responses. Physiologic and/or pharmacologic MRI can greatly help define the dose and schedule of treatments used for lung cancers, pleural effusions resulting from treatments and induction of cytokine overexpression, syndromes such as asthma or other immunologic compromises of the lung, and many more similar pathologies. The air spaces of the lung can create very large magnetic susceptibility artifacts and it has traditionally been very difficult to image small structures (like nascent tumors) accurately. Using MR techniques that reduce the image sensitivity to susceptibility diphase such as spin-echo variants can yield image clarity which is competitive with CT detection. This enables lung parenchymal imaging and makes MRI somewhat competitive with X-ray CT in these applications (Stolzmann et al. 2013).

DWI techniques can be used to observe image changes in tissue with such as carcinoma or tumor heterogeneity by changes in the diffusion sensitivity. These techniques can produce a secondary and confirmatory contrast for other techniques that depend on discrimination via T_1 or T_2 changes. This use of ADC has been shown to be a good marker for radiosensitivity as this generally tracks the hypoxic environments in tumors (Williams et al. 2013). The use of ADC without the use of contrast agent provides a stable longitudinal biomarker for therapeutic evaluation without complications due to imaging timing or animal preparation. Likewise ADC DWI can be used to determine rapidly occurring changes due the tumor vascularity and changes due to angiotensive factors producing disordered vascular permeability. Figure 11.10 below shows the ADC tracking changes in glioma growth model in

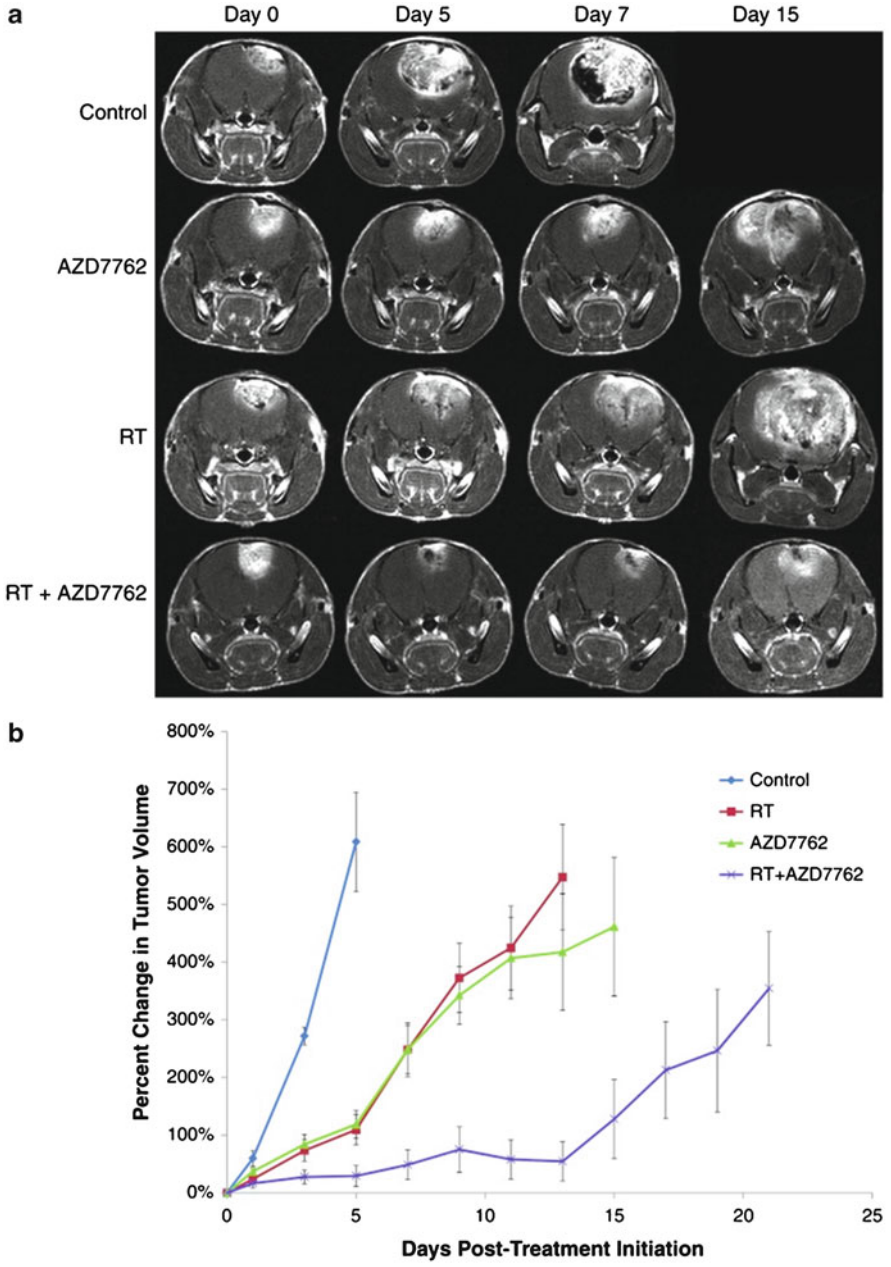

Fig. 11.10 MR images of rat cerebral tumors and treatment response. (**a**) MRI data consist of anatomic contrast-enhancing coronal T_1-weighted images for representative animals from each of the treatment groups from pretreatment (day 0) to days 5, 7, and 15. Day 15 is not shown for the control animal due to the rapid tumor growth for untreated animals. (**b**) MRI-determined intracerebral tumor volumes over time for each treatment group. Treatments occurred for 10 days total, 5 days/week. MRI was performed every other day during treatment and thereafter to determine tumor volume until end of study period for (1) control ($n=7$), (2) 15 mg/kg AZD7762 ($n=10$), (3) RT ($n=10$), or (4) AZD7762+RT ($n=12$). Error bars represent SEM. All tumor volumes were significantly different ($P<0.05$) from control tumor volumes beginning at day 3 post-treatment initiation. The combined therapy group was also significantly different ($P<0.05$) from the other three groups beginning at day 3 post-treatment initiation. Reproduced from: Williams et al. (2013) with permission

rodents with and without the administration of a radiosensitivity agent (i.e., selectively sensitizing tumors to DNA-damaging agents, kinase inhibitors).

Other related changes to the tumor environment such as perfusion can be detected via MRI. These perfusion-weighted imaging techniques can be used to determine the standard Kety equation parameters for bulk blood flow into tissue with quantification that is similar to PET 18-O-H_2O measurements. Quantified perfusion measurements via arterial spin labeling (ASL) techniques require additional time for the perfused spins to exchange with the tumor vascular bed and ECF (Wolf et al. 2005).

Other pulse sequences may find other applications in oncology as they can help to detect signal-loss image artifacts in the vicinity of other potentially attenuating structures such as iron-rich sites of necrosis or hemorrhage which are relatively common in tumors. The technique known as susceptibility-weighted imaging (SWI) is quite sensitive for detecting the changes that occur from necrosis and hemorrhage (Mittal et al. 2009). SWI, a post processing technique, detects the small local magnetic fields that distort the MRI signal phase on very short distance scales while retaining the high SNR of a standard gradient echo MRI.

11.4 Quality Control, Noise, Performance Monitoring, Contrast-to-Noise Ratio (CNR)

11.4.1 Noise and Artifacts in MRI

Noise and artifacts are part of the landscape of any analytical system. MRI has many that are intrinsic and many that are outside of the instrument and can be, in part, controlled by the operator and through environmental forethought in the design of the laboratory. There are additive elements of noise in MRI. These include thermal noise from the body which is the summation of thermal vibration of ions, electrons, etc., and this is the dominant noise in most MRI systems. There is also simple digital quantized noise from the analog to digital (A/D) devices and controllers, preamplifiers, and other sources of electronic noise. The RF coils have their own inherent thermal noise. A/D devices, preamps, and electronic noise and thermal noise in the RF coils are more limiting factors for very small objects such as for MRI microscopy. The use of higher fields is usually intended to achieve higher SNR, but this is dependent on the pulse sequence and the relaxation properties of the system being imaged; higher fields can sometimes reduce the SNR especially if the pulse sequence relies on prolonged periods of transverse magnetization such as in EPI. Major sources of nonthermal noise or variation in fMRI include cardiac and pulmonary variations, head movement, low-frequency noise, spontaneous neural and vascular fluctuations (BOLD noise), and behavior variations (subject and system). Sources of variation generally become more significant with increasing field strength. If one wants lower spatial resolution, then the thermal noise elements become less significant. Temporal

noise is also something that should be considered and is mostly related to time of day, system operating times (durations), variations in system support (heating, environmental controls cycling, HVAC, electrical power loads), and other variables.

In fMRI, Geissler et al. (2007) suggest that the contrast-to-noise ratio (CNR) may be a useful quality check. The contrast-to-noise ratio (CNR) is directly linked to statistical measures such as the *t*-values, but it does not depend on the number of points or number of runs (scans) as do the *t*-values themselves. In fMRI, the CNR is made up of the functional signal change and the temporal signal change as the average signal change (task related) over the non-task-related variability over time (time-series noise). The CNR is thus a useful intuitive parameter to estimate fMRI performance and may be useful in comparing fMRI images across imaging sessions and potentially across institutions.

11.4.2 ACR Practice Guidelines and Medical Physics Performance Monitoring

The American College of Radiology (ACR) has published Guidelines on MRI equipment and on performance standards for the performance and interpretation of MRI imaging (ACR 2003; ACR 2004). The Medical Physics Performance document (2004) sets goals for performance to produce consistency of the MR instrumentation and associated peripherals. They suggest the following performance characteristics be monitored:

- Physical and mechanical inspection
- Phase stability
- Magnetic field homogeneity
- Magnetic field gradient calibration
- Radiofrequency (RF) calibration for all coil
- Image signal-to-noise ratio (SNR) for all coils
- Intensity uniformity for all volume coils
- Slice thickness and location accuracy
- Spatial resolution and low contrast object detectability
- Artifact evaluation
- Film processor quality control (if applicable)
- Hard copy fidelity
- Soft copy fidelity
- MRI safety checks—environmental postings and controls

In addition, they recommend the following quality control programs for fMRI (and by association MRI in general):

- Physical and mechanical inspections
- Magnetic field gradient calibration
- RF calibration for the head coil (in fMRI, and brain imaging)
- Image SNR and uniformity for the head coil

- Film processor QC
- Hard and soft copy fidelity

Initial performance checks should be performed on installation and more comprehensive that the annual and the period performance checks. Acceptance testing should include the evaluation of all coils with reproducible but realistic phantom subjects since coil performance depends on the size, position, and conductivity of the sample. It must be clear that the peripherals are often not associated with the quality program and as such often are weak links in image quality and interpretation and may lead to errors in image evaluations. For systems of MRS (spectroscopy) an MRS series of quality checks in addition to these are recommended. The reader is directed to Chap. 12 on MRS techniques for further information.

The ACR Guidance for Performing and Interpreting MRI (2003) defines the staffing and training requirements (incl. medical physicists), technologists, and others. In addition, the document serves to guide the requirements on system documentation, equipment specifications, safety guidelines, quality control programs, and also such topics as infection control and imaging subject education and allowances for concerns (Kanal et al. 2013).

Friedman and Glover (2006) have provided an excellent review on approaches they have observed and recommend for multicenter fMRI quality assurance protocols. fMRI acquisitions are highly dependent on temporal stability. BOLD signals are changes on only a few percent in magnitude, and as such thermal or environmental change can affect the system and wipe out collected data by simply added noise. Stability across days, weeks, and months is necessary for fMRI systems. Friedman and Glover provide specific examples of what they term FIRST-BIRN fMRI and they provide sequence parameters using EPI or "spiral gradient echo recalled" (see Table 11.1 in Sect. 1.1). The authors of the paper discuss the phantom used in the Glover stability QA protocol as a 17 cm diameter spherical plastic vessel (Dielectric Inc., Madison, WI) filled with a doped agar gel designed to approximate the brain in terms of T_1 and RF conductivity. The reader is encouraged to review their paper and develop familiarity with their approaches.

11.5 Conclusions

MRI technology continues to develop in ways that make it more available and more relevant to the drug and biologics development laboratory. As it moves from "nice to have" to being an essential readout, it will have a significant impact on the way we approach regulatory approvals and it will be an incredibly versatile part of the investigative "tool chest" of development, not unlike what PCR did to molecular biology.

Oncology, psychopharmacology, physiologic and pharmacologic MR (phMRI) intervention, stroke, and many other applications and investigative approaches of MR are available to the drug and biologics drug development teams. It is the

application of this extraordinarily versatile imaging modality that can deliver both anatomy and function that has added major new avenues of noninvasive imaging toward understanding of the complexities of biology. It is expected that MRI will be one of the most accessible imaging technologies used in drug and biologic development.

The uses and image value of MRI are only as good as the quality checks and performance standards that are executed. There are primary quality control checks that are important to remain diligent. It is possible that use of the contrast-to-noise ratio (CNR), especially for fMRI (Sorenson 2006), may help serve as a uniform quality check that can work across studies and even across institutions.

Contrast agents are available, but they must be administered in high concentrations that can be toxic in some individuals who are compromised by pathologies affecting hepatic or renal function. Gd, Dy, and Mn are the important paramagnetic elements employed in commercial contrast agents for MR imaging. These agents are not the image "content" post-administration as is common of CT and X-ray imaging, but rather their *effects* on tissue water relaxivity is what actually creates the image. It is important, especially for Gd ions, to remain caged within the chelate structure to avoid an associated nephrogenic systemic fibrosis which is generally observed in the elderly and especially in renal disease with reduced clearance capacity.

References

ACR practice guideline: performing and interpreting MRI, ACR technical standard for performing and interpreting magnetic resonance imaging (MRI), 1992 (Res 14), amended 1995, 96, 2000, 2001, 2002, effective 1/1/2003, pp 29–33

ACR technical standard: MRI equipment, ACR technical standard for diagnostic medical physics performance monitoring of magnetic resonance imaging (MRI) equipment, 1999 (Res 19), revised 2004 (Res 17b), pp 743–745

Becerra L, Upadhyay J, Chang P-C et al (2013) Parallel buprenorphine phMRI responses in conscious rodents and healthy human subjects. J Pharmacol Exp Ther 345:41–51

Buxton RB (2002) Introduction to functional magnetic resonance imaging: principles and techniques. Cambridge University Press, Cambridge. Second revised edition published in October 2009

Buxton RB (2010) Interpreting oxygenation-based neuroimaging signals: the importance and the challenge of understanding brain oxygen metabolism. Front Neuroenergetics 2:8

Cory DA, Schwartzentruber DJ, Mock BH (1987) Ingested manganese chloride as a contrast agent for magnetic resonance imaging. Magn Reson Imaging 5(1):65–70

Damadian R, Goldsmith M, Minkoff L (1977) NMR in cancer: XVI. FONAR image of the live human body. Physiol Chem Phys 9:97–100

D'Esposito M, Deouell LY, Gazzaley A (2003) Alterations in the BOLD fMRI signal with ageing and disease: a challenge for neuroscience. Nat Rev Neurosci 4:863–872

Faulkner W (2008) Gadolinium based contrast agents. SMRT Educ Sem 11(2):5–10

Ferrari L, Turrini G, Crestan V, Bertani S, Cristofori P, Bifone A, Gozzi A (2012) A robust experimental protocol for pharmacological fMRI in rats and mice. J Neutrosci Methods 204:9–18

Friedman L, Glover GH (2006) Report on a multicenter fMRI quality assurance protocol. J Magn Reson Imaging 23:827–839

Gavin PR, Bagley RS (eds) (2009) Practical small animal MRI. Wiley-Blackwell, Ames, IA

Geva T (2006) Magnetic resonance imaging: historical perspective. J Cardiovasc Magnet Reson 8:573–580
Geissler A, Gartus A, Foki T, Tahamtan AR, Beisteiner R, Barth M (2007) Contrast-to-Noise ratio (CRN) as a quality parameter in fMRI. J Magn Reson Imaging 25:1263–1270
Hustvedt SO, Grant D, Southon TE, Zech K (1997) Plasma pharmacokinetics, tissue distribution and excretion of MnDPDP in the rat and dog after intravenous administration. Acta Radiol 38 (4 Pt 2):690–699
Jensen JH, Helpern JA, Ramani A, Lu H, Kaczynski K (2005) Diffusional kurtosis imaging: the quantification of non-gaussian water diffusion by means of magnetic resonance imaging. Magn Reson Med 53:1432–1440
Kanal E (2008) Nephrogenic syndrome fibrosis. SMRT Educ Sem 11(2):11–14
Kanal E, Expert Panel on MR Safety et al (2013) ACR guidance document on MR safe practices. J Magn Reson Imaging 37:501–530
Kirchin MA, Runge VM (2008) Contrast agents for magnetic resonance imaging: safety update. SMRT Educ Sem 11(2):15–23
Krupnick AS, Tidwell VK, Engelbach JA, Alli VV, Nehori A, You M, Vikis HG, Gelman AE, Kreisel D, Garbow JR (2012) Quantitative monitoring of mouse lung tumors by magnetic resonance imaging. Nat Protoc 7(1):128–142
Lauterbur PC (1973) Image formation by induced local interactions: examples employing nuclear magnetic resonance. Nature 242:190–191
Logothetis NK, Wandell BA (2004) Interpreting the BOLD Signal. Annu Rev Physiol 66: 735–769
Matthews PM, Honey GD, Bullmore ET (2006) Applications of fMRI in translational medicine and clinical practice. Nat Rev Neurosci 7:732–744
Mendonca-Dias MH, Gaggelli E, Lauterbur PC (1983) Paramagnetic contrast agents in nuclear magnetic resonance medical imaging. Semin Nucl Med 13(4):364–376
Miller KL, Luh WM, Liu TT, Martinez A, Obata T, Wong EC, Frank LR, Buxton RB (2001) Nonlinear temporal dynamics of the cerebral blood flow response. Hum Brain Mapp 13:1–12
Mittal S, Wu Z, Neelavalli J, Haacke EM (2009) Susceptibility-weighted imaging: technical aspects and clinical applications, part 2. AJNR Am J Neuroradiol 30:232–252
Mitterschiffthaler MT, Ettinger U, Mehta MA, Mataix-Cols D, Williams SCR (2006) Applications of functional magnetic resonance imaging in psychiatry. J Magn Reson Imaging 23:851–861
Moseley ME, Liu C, Rodriguez S, Brosnan T (2009) Advances in magnetic resonance neuro-imaging. Neuro Clin 27:1–19
Neil JJ (2008) Diffusion imaging concepts for clinicians. J Magn Reson Imaging 27:1–7
Paschal CB, Morris HD (2004) K-space in the clinic. J Magn Reson Imaging 19:145–159
Rivkin MJ (2000) Developmental neuroimaging of children using magnetic resonance techniques. Ment Retard Dev Disabil Res Rev 6:68–80
Roe AW, Chen LM (2008) High resolution fMRI maps of cortical stimulation in nonhuman primates: correlation with intrinsic signal optical images. ILAR J 49(1):116–123
Schepkin VD, Brey WW, Gor'kov PL, Grant SC (2010) Initial in vivo rodent sodium and proton MR imaging at 21.1 T. Magn Reson Imaging 28:400–407
Schlaug G, Stewart B, Benfield A, Edelman RR, Warach S (1997) Time course of the apparent diffusion coefficient (ADC) abnormality in human stroke. Neurology 49(1):113–119
Sorenson AG (2006) Future prospects for fMRI in the clinic. J Magn Reson Imaging 23:941–944
Stolzmann P et al (2013) Detection rate, location, and size of pulmonary nodules in trimodality PET/CT-MR. Invest Radiol 48:241–246
Thomsen HS, Loegager V, Noerrgaard H, Chabanova E, Moller J, Sonne J (2005) Oral manganese for liver and bile imaging. Acad Radiol 12(Suppl 1):S21–S23
Toft KG, Hustvedt SO, Grant D et al (1997) Metabolism and pharmacokinetics of MnDPDP in man. Acta Radiol 38(4 Pt 2):677–689
UCSD, Center for Functional MRI, why is the MR signal sensitive to changes in brain activity? http://fmri.ucsd.edu/Research/whatisfmri.html. Accessed 13 May 2013

UK (2005) (now in 4th edition, 2011: http://www.westbrookmriinpractice.com/)
Westbrook C, Roth CK, Talbot J (2011) MRI in practice, 3rd edn. Blackwell, Oxford
Williams TM et al (2013) DW-MRI as a predictive biomarker of radiosensitization of GBM through targeted inhibition of checkpoint kinases. Transl Oncol 6:133–142
Wise RG, Tracey I (2006) The role of fMRI in drug discovery. J Magn Reson Imaging 23: 862–876
Wolf RL et al (2005) Grading of CNS neoplasms using continuous arterial spin labeled perfusion MR imaging at 3 Tesla. J Magn Reson Imaging 22:475–482
Yang GY, Betz AL (1994) Reperfusion-induced injury to the blood-brain barrier after middle cerebral artery occlusion in rats. Stroke 25:1658–1664
Young RJ, Knopp EA (2007) Brain MRI: tumor evaluation, in, update: MRI of the brain. SMRT Educat Sem 10(4):23–38
Yurgelun-Todd DA, Coyle JT, Gruber SA, Renshaw PF, Silveri MM, Amico E, Cohen B, Goff DC (2005) Functional magnetic resonance imaging studies of schizophrenic patients during word production: effect of D-cycloserine. Psychiatry Res 138:23–31